

**Systemic and Tumor-targeted Delivery of siRNA by Cyclic
NGR and isoDGR Motif-containing Peptides**

Journal:	<i>Biomaterials Science</i>
Manuscript ID	BM-ART-10-2015-000429.R2
Article Type:	Paper
Date Submitted by the Author:	29-Dec-2015
Complete List of Authors:	Huang, Yuanyu; Peking University, Institute of Molecular Medicine Cheng, Qiang; Peking University, Jin, Xingyu; Suzhou Ribo Life Science Co. Ltd., Ji, Jia-Li; Suzhou Ribo Life Science Co. Ltd., Guo, Shutao; National Center for Nanoscience and Technology of China, Zheng, Shuquan; Peking University, Wang, Xiaoxia; Peking University, Cao, Huiqing; Peking University, Gao, Shan; Suzhou Ribo Life Science Co. Ltd., Liang, Xing-Jie; National Center for Nanoscience and Technology of China, Du, Quan; Peking University, Liang, Zicai; Peking University,

Systemic and Tumor-targeted Delivery of siRNA by Cyclic NGR and *iso*DGR Motif-containing Peptides

Yuanyu Huang^{1*}, Qiang Cheng¹, Xingyu Jin⁴, Jia-Li Ji⁴, Shutao Guo², Shuquan Zheng¹,
Xiaoxia Wang¹, Huiqing Cao¹, Shan Gao⁴, Xing-Jie Liang², Quan Du^{1*}, Zicai Liang^{1,3*}

¹ Institute of Molecular Medicine; State Key Laboratory of Natural and Biomimetic Drugs, School of Pharmaceutical Sciences; Peking University, Beijing 100871, China

² Chinese Academy of Sciences Key Laboratory for Biomedical Effects of Nanomaterials and Nanosafety, National Center for Nanoscience and Technology of China, Beijing 100190, China

³ Collaborative Innovation Center of Chemical Science and Engineering (Tianjin), Tianjin 300072, China

⁴ Suzhou Ribo Life Science Co. Ltd., Jiangsu 215300, China

* Correspondence should be addressed to Y. Huang (yyhuang@pku.edu.cn, Tel: +86-10-62750683), Z. Liang (liangz@pku.edu.cn, Tel./fax: +86-10-62769862) or Q. Du (quan.du@pku.edu.cn, Tel./Fax: +86-10-82805780).

Abstract

The drug development of siRNA has been seriously hindered by the lack of an effective, safe and clinically applicable delivery system. The cyclic NGR motif and its isomerization product *iso*DGR recruit CD13 and integrin as their specific receptors, both of which are overexpressed by tumor and neovascular cells. In this study, a bi-functional peptide, named NGR-10R, was designed and tested for siRNA delivery *in vitro* and *in vivo*. Through the formation of peptide/siRNA nanoparticles, RNase resistance was greatly enhanced for the siRNAs. Both FACS and confocal assays revealed that the peptide/siRNA complexes were effectively internalized by MDA-MB-231 cells. Gene silencing assays indicated that anti-Lamin A/C siRNA delivered by NGR-10R robustly repressed gene expression in MDA-MB-231 and HUVEC (a CD13⁺/α_vβ₃⁺ cell). Importantly, the siRNAs were efficiently delivered into tumor tissues and localized around the nuclei, as revealed by *in vivo* imaging and cryosection examination. In summary, NGR-10R not only efficiently delivered siRNAs into MDA-MB-231 cells *in vitro* but also delivered siRNAs into tumor cells *in vivo*, taking advantage of its specific binding to CD13 (neovascular) or α_vβ₃ (MDA-MB-231). Therefore, the NGR-10R peptide provides a promising siRNA delivery reagent that could be used for drug development, particularly for anti-tumor therapeutics.

Introduction

RNA interference (RNAi) enables efficient target gene silencing *via* transcript cleavage. Taking advantage of this specific and potent endogenous mechanism, small interfering RNAs (siRNAs) are generally used in both basic research and drug development, particularly for genetic diseases, virus infection, cancer, metabolic disease and immunological diseases. Recently, promising clinical studies have been reported ¹⁻⁵. However, because of its large molecular size and negative-charged property, it is difficult for siRNA by itself to penetrate the cell membrane to trigger RNAi. The lack of an efficient, safe and clinically applicable delivery reagent has seriously hindered the clinical application of siRNAs.

Cell penetration peptides (CPPs) are generally used to deliver conjugated bioactive cargoes into cells or even tissues, primarily *via* endocytosis. Virus-derived CPPs are the most investigated, exhibiting robust cell penetration and gene delivery capacity. The trans-activating transcriptional activator peptide, TAT, was the first CPP identified in human immunodeficiency virus 1 (HIV-1) in 1988 and can efficiently deliver gene products into cells ⁶. However, potential risks resulting from their immunogenicity severely limited their clinical practice. Therefore, non-virus-derived CPPs, which mediate receptor-facilitated endocytosis, provide another possibility for drug development.

The Asn-Gly-Arg (NGR) motif-containing peptide was discovered by Ruoslahti E. and colleagues ⁷ using phage display technology. Earlier studies observed that this peptide specifically binds to the tumor vasculature, and it was successfully used to deliver doxorubicin into tumor cells (MDA-MB-435 and MDA-MB-231). Its tumor-targeting ability

relies on its specific interaction with CD13 (aminopeptidase N), which is selectively overexpressed in neovascular and some tumor cells and seldom expressed in quiet vascular endothelial cells⁸⁻¹⁰. Taking advantage of its tumor-targeting property, NGR motif-containing peptides were used to facilitate therapeutic reagent delivery, enhance their antineoplastic effects or reduce their application dose¹¹. For instance, both cyclic and linear forms of NGR-containing peptides have been used to assist clinical imaging diagnosis¹² or facilitate the delivery of multiple drugs, including tumor necrosis factor (TNF)¹³⁻¹⁶, interferon (IFN)¹⁷⁻²⁰, tissue factor²¹, virus env escort proteins²², liposome-encapsulated doxorubicin^{23, 24} and other chemotherapeutic or anti-angiogenesis molecules²⁵⁻²⁷. An antitumor recombinant protein, CNGRC peptide-TNF alpha conjugate, termed NGR-hTNF, is currently undergoing Phase III clinical trials for the treatment of malignant pleural mesothelioma caused by exposure to asbestos^{28, 29}. NGR-hTNF is also being investigated, alone or in combination with chemotherapy on four different solid tumors in four other randomized Phase II trials³⁰⁻³⁴. Moreover, another fusion protein tTF-NGR consisting of the extracellular domain of the thrombogenic human tissue factor (truncated tissue factor, tTF) and the peptide GNGRAHA (NGR) is currently undergoing a Phase I clinical trial^{21, 35, 36}.

Asn deamidation is a well-known phenomenon that exists extensively in biological and chemical processes. The Asn residues, particularly when followed by Gly, can undergo thermodynamically-spontaneous and non-enzymatic deamidation *via* succinimide intermediate at physiological pH^{37, 38}, leading to formation of aspartic acid (Asp, D) or *iso*-aspartic acid (*iso*Asp, *iso*D), predominantly in L-configuration. The deamidation of Asn in the NGR motif occurs *via* loss of ammonia (-17 Da) followed by hydrolysis of the succinimide

ring (+18 Da) with a global gain of +1 Da³⁹. This reaction can occur *in vivo*, e.g. in extracellular matrix proteins with slow turnover, and *in vitro* during protein isolation and storage. The presence of a Gly residue after Asn has a dramatic destabilizing effect³⁸. Accordingly, the kinetics of NGR deamidation in synthetic fibronectin (FN) fragments and peptides are surprisingly rapid³⁹. The half-life of NGR-2C (with an amino acid sequence of CNGRCGVRY) at pH 7.53 and pH 8.50 was ~4 and ~2 h, respectively³⁹. The maximal competitive binding activity of CNGRC-TNF (consisting of murine TNF fused with the C terminus of CNGRCG) to $\alpha_v\beta_3$ with FN-I₅ was reached at 24-48 h (with a half-life of 3.4 h)³⁹. Fibronectins are large glycoproteins (~450 kDa) composed of two nearly identical disulfide-bonded subunits. Each subunit consists of three types of repeating homologous modules termed FN-I, FN-II, and FN-III repeats. FN-I₅ is a repeating homologous module that contains a GNGRG loop. It was also observed that CNGRC-TNF could, to some extent, bind to $\alpha_v\beta_3$ even before being treated with an accelerated deamidation process, possibly due to deamidation occurring during preparation and/or assay incubation³⁹. The non-enzymatic process results in the loss of affinity between NGR and CD13. Instead, the product of asparagine deamidation, cyclic *iso*DGR, is able to interact with integrins by recognition of the RGD (Arg-Gly-Asp)-binding site of several integrins, including $\alpha_v\beta_3$ ^{14, 40}. Integrin $\alpha_v\beta_3$ and $\alpha_v\beta_5$ are also overexpressed in tumor and neovascular cells⁴¹. Hence, the NGR-to-*iso*DGR transition can lead to CD13/integrin receptor switching. However, linear NGR peptides mainly undergo degradation reactions involving the alpha-amino group, which generates non-functional six/seven-membered ring compounds, which are unable to bind $\alpha_v\beta_3$, and a small amount of *iso*DGR⁴². The affinity of cyclic *iso*DGR binding to $\alpha_v\beta_3$ is more

than 100-fold higher than that of linear *iso*DGR. Cyclic *iso*DGR can also bind to other integrins ($\alpha_v\beta_5$, $\alpha_v\beta_6$, $\alpha_v\beta_8$ and $\alpha_5\beta_1$) but with 10-100-fold lower affinity than with $\alpha_v\beta_3$. In addition to the generation of high binding affinity with integrins, the disulfide linkage between the two cysteines further enhances its tumor targeting ability and configuration stability⁴³. Moreover, the RGD motif may activate the conformational changes of the integrin, resulting in initiation of unwanted signaling pathway, which may induce undesirable effects including receptor clustering, activation and redistribution. However, it has been demonstrated that the *iso*DGR-containing cyclopeptides are true $\alpha_v\beta_3$ antagonists unable to stimulate integrin accumulation at the cell edge, and will not induce agonist-like activities and adverse paradoxical effects⁴⁴. Collectively, Asn deamidation is a thermodynamically spontaneous reaction independent from enzymatic regulation, benefiting from which, cyclic NGR motif-containing peptides exhibit both CD13 and integrin binding capacity, which makes them ideal tumor-targeting ligands.

Recently, Hou L *et al.*⁴⁵ investigated the antitumor activity of CDAK, a *Ciso*DGRC-containing antimicrobial peptide, in MCF-7 and MDA-MB-231 cell lines. These two cell lines were observed to be CD13 negative and $\alpha_v\beta_3$ positive (CD13⁻/ $\alpha_v\beta_3$ ⁺). Their study demonstrated that CDAK induced apoptosis and inhibited the proliferation of cancer cells through S phase arrest in the cells. In addition, CDAK inhibited the invasion of MDA-MB-231 *in vitro* and significantly repressed the progression of the tumor and the generation of neovascularization *in vivo*. However, only a few works have been reported on its application in siRNA delivery to date. NGR peptide was employed only as a targeting moiety of the whole delivery system in the previous studies^{46, 47}. The pivotal components of the delivery

systems were the other materials, such as polyethylenimine (PEI)-functionalized single-walled carbon nanotubes⁴⁶ or PEGylated LPD (liposome-polycation-DNA) nanoparticles⁴⁷. In addition, these studies focused mainly on the scenario of NGR-CD13 by investigating siRNA transfection in CD13-positive (CD13⁺) cells, and few paid attention to the property of NGR-*iso*DGR- $\alpha_v\beta_3$ that assisted siRNA transportation in CD13⁻/ $\alpha_v\beta_3$ ⁺ cells, let alone the script that applied a single component NGR peptide itself to deliver siRNA in CD13⁻/ $\alpha_v\beta_3$ ⁺ cells.

In this study, NGR-10R, a cyclic NGR motif-containing peptide with an amino acid sequence of CNGRCGRRRRRRRRRR (from the N terminal to the C terminal), was designed and synthesized. The two cysteines were linked with a disulfide bond. CNGRCG on the N terminal is the targeting moiety, and polyarginine (10R) on the C terminal was designed to bind siRNA through electrostatic interaction. To explore (i) whether siRNAs could be transfected into MDA-MB-231, a CD13⁻/ $\alpha_v\beta_3$ ⁺ cell line, by NGR-10R *in vitro*, (ii) if siRNAs could further result in robust gene silencing, (iii) the biodistribution profile of NGR-10R/siRNA complexes after being intravenously injected into the mice, and (iv) the *in vivo* tumor-targeting properties of NGR-10R/siRNA complexes, a series of assays including gel retardation assay, RNase resistance assay, MTT, fluorescence activated cell sorting (FACS), confocal laser scanning microscopy (CLMS), real-time quantitative polymerase chain reaction (RT-qPCR), Western blotting, *in vivo* fluorescent imaging, and cryosection examination were performed.

Experimental section

Materials

NGR-10R, with an amino acid sequence of CNGRCGRRRRRRRRRR, a molecular formula of $C_{80}H_{154}N_{50}O_{18}S_2$, and a molecular weight of 2168.57 g/mol, was synthesized by Invitrogen (USA) (supplementary figure S1). The purity identified by HPLC was 97.46 %. Polyarginine (10R) was purchased from Beijing SciLight Biotechnology Ltd. Co. (Beijing, China). The arginines of both the NGR-10R and 10R peptides were L-form amino acids. RVG-9dR, with an amino acid sequence of YTIWMPENPRPGTPCDIFTNSRGKRASNGGGGRRRRRRRRR, was also provided by Invitrogen (USA). The C-terminal arginines of RVG-9dR were D-form amino acids. The reverse-transcription kit and all the reagents used in the real-time quantitative PCR were purchased from TIANGEN Biotech (Beijing) Co., Ltd. (Beijing, China). Sybr Green was purchased from Invitrogen (USA). Lamin A/C monoantibody and horseradish peroxidase (HRP)-labeled goat anti-rabbit secondary antibody were purchased from Cell Signaling Technology, Inc. (Danvers, MA, USA) and Bio-Rad Laboratories (Hercules, CA, USA), respectively. GAPDH antibody and DAPI (4', 6-diamidino-2-phenylindole) were provided by Zhongshan Goldenbridge Biotechnology Co. Ltd. (Beijing, China). The commercial transfection reagents lipofectamineTM 2000 and X-TremeGENE were purchased from Invitrogen (USA) and Roche (Basel, Switzerland), respectively. FAM-labeled NC siRNA, si-NC67-M, mmu-miR-672, and siLamin A/C were provided by Shanghai GenePharma Co., Ltd. (Shanghai, China). Cy5-labeled NC siRNA was supplied by Suzhou Ribo Life Science Co., Ltd. (Kunshan, China). Their sequences were as follows: FAM-labeled NC siRNA: sense strand: 5'-FAM-CCUUGAGGCAUACUUCAAAdTdT-3', the

labeling of fluorophore FAM was made at 5' of the sense strand; antisense strand:

5'-UUUGAAGUAUGCCUCAAGGdTdT- 3'. si-NC67-M: sense strand:

5'-UCACAACCUCCUAGAAAGAGUAGA-3'; antisense strand:

5'-UACUCUUUCUAGGAGGUUGUUAUU-3'. mmu-miR-672: sense strand:

5'-UGAGGUUGGUGUACUGUGUGUGA-3'; antisense strand:

5'-ACACACAGUACACCAACCUUAUU-3'. siLamin A/C: sense strand:

5'-CUGGACUCCAGAAGAACAAdTdT-3'; antisense strand:

5'-UGUUCUUCUGGAAGUCCAGdTdT- 3'. Cy5-labeled NC siRNA: sense strand:

5'-Cy5-CCUUGAGGCAUACUCAAAdTdT-3', the fluorophore Cy5 was also labeled at 5' of

the sense strand; antisense strand: 5'-UUUGAAGUAUGCCUCAAGGdTdT- 3'. Moreover, to

stabilize the sequence and enable it to resist RNase attack, certain bases of Cy5-NC siRNA

were modified with 2'-Ome or fluoro.

Preparation of NGR-10R/siRNA complexes

According to the requirements of the indicated experiment, NGR-10R powder was dissolved into 200–1000 μM (approximately 0.60–3.0 $\mu\text{g}/\mu\text{l}$) (for the *in vitro* testing) or 10–30 $\mu\text{g}/\mu\text{l}$ (for the *in vivo* study) with diethylpyrocarbonate (DEPC)-treated water. Meanwhile, siRNA was dissolved into 20 μM ($\sim 0.266 \mu\text{g}/\mu\text{l}$) or 1 $\mu\text{g}/\mu\text{l}$ with DEPC water for *in vitro* tests or *in vivo* studies, respectively. Peptide and siRNA solutions were mixed directly according to different desired molar ratios. After electrostatic interaction for 15–20 min at room temperature, peptide/siRNA complexes were formed (Scheme 1a). Additional DEPC water or 1 \times PBS or

normal saline (NS) could be added into the complexes to obtain the final transfection or administration solution.

Gel retardation assay

A gel retardation assay was used to evaluate the siRNA loading capability of NGR-10R. Here, si-NC67-M, a serum-stable siRNA⁴⁸, was used to prepare the peptide/siRNA complexes according to the above-mentioned protocol. Twenty-two point five microliter complexes containing 50 pmol siRNAs (20 μ M, 2.5 μ l) were mixed with four microliter 6 \times loading buffer and then loaded into a 4 wt % agarose gel containing 5 μ g/ml ethidium bromide (EB), followed by separating for 40 min in 1 \times TAE buffer at 120 V and finally exposure with a UV illuminator.

RNase resistance

An RNase-resistance assay was performed to verify whether NGR-10R could protect siRNA from RNase attack. The small RNA selected in this test was mmu-miR-672. There is a small RNA library in our lab, which includes hundreds of siRNAs and microRNAs. Previously, we comprehensively analyzed the sequence-specific stability of small RNA⁴⁹, providing several rational modification strategies to stabilize small RNA. According to their degradation patterns, small RNAs were divided into four categories: stable, semistable, hypostable and nonstable. mmu-miR-672 is a representative nonstable small RNA. The nucleotide base constituents (cytosine, guanine, adenine and uracil) and physico-chemical properties

(double strand, 19-25 nt) of chemical-synthetic siRNA and miRNA are almost identical. Biologically, it has been demonstrated that siRNAs could work like miRNAs, and not all miRNAs work by binding with imperfect complementarity to mRNAs and preventing their translation (miRNAs could also repress gene expression in the way of siRNAs)⁵⁰. Therefore, we believe that Rnase resistance data collected with unstable mmu-miR-672 are convincing, particularly because this assay aims to elaborate the stability issue, not the biological issue.

NGR-10R/RNA complexes containing 22.5 pmol mmu-miR-672 were prepared at a molar ratio of 100:1. An equal amount of naked mmu-miR-672 solution with the same volume of NGR-10R/RNA complexes was also prepared. Peptide/RNA complexes and naked mmu-miR-672 were incubated in 10 % FBS (v/v, mixed with 1×PBS) at 37 °C. Then, samples were collected and immediately frozen at -20 °C at 0, 3, 6 and 12 h, respectively. Then, all the solutions were centrifuged for 5 min at 10000 rpm and 4 °C to precipitate complexes and naked RNA. The supernatants were discarded, and 15 µl of DEPC water was added to resuspend the precipitate. To destroy the complexes and release the RNA, proteinase K (0.2 µl, 1 mg/ml), Tris-HCl (1 µl, 50 mM, pH = 7.0) and CaCl₂ (1 µl, 5 mM) were added into the resuspended complexes solution, followed by incubating for an additional 4–5 h at 37 °C. After adding loading buffer, all the solutions were separated in native 20 % polyacrylamide gel electrophoresis (PAGE) for 150 min at a constant voltage of 150 V. Finally, the gels were stained with Sybr Gold for 20 min, exposed by a Vilber Lourmat imaging system (France) and analyzed with Biocap software to show the location of the small RNA.

Physicochemical property characterization

The particle size and zeta potential of peptide/siRNA complexes were measured with a Zetasizer 3000HS (Malvern Instruments, Inc., Worcestershire, UK) at a wavelength of 677 nm with a constant angle of 90° at room temperature. The complexes were prepared by mixing 2 µg si-NC67-M (7.69 µl, 20 µM) and the required amount of peptide (1000 µM) and incubating for 15–20 min at room temperature. The solutions were then diluted with 0.8 ml of double-distilled water before being analyzed with a Zetasizer 3000HS. In addition, the morphology and size of the complexes were further investigated using transmission electron microscopy (TEM) (Tecnai G2 20 STWIN transmission electron microscope, Philips, Netherlands) with a 200-kV acceleration voltage. Briefly, the samples were prepared by dipping 7 µl of the complexes solution onto a carbon-coated copper grid, followed by negatively staining with 1 % (wt/v) phosphotungstic acid (adjusted pH to 7.3 with 1 N NaOH) and air-drying before acquiring TEM images.

Cells

MDA-MB-231, a breast carcinoma cell line, was obtained from the Cell Resource Center of Peking Union Medical College (Beijing, China). The cells were cultured with L15 medium supplemented with 10 % fetal bovine serum, 100 units/ml penicillin and 100 µg/ml streptomycin at 37 °C in a 100 % air humidified atmosphere (without CO₂). CO₂ was blanked off by twinning the culture plates or bottles with parafilm. Human umbilical vein endothelial cells (HUVECs) were grown in medium 199 (Invitrogen) containing fibroblast growth factor,

heparin and 20 % fetal bovine serum (Hyclone, Ogden, UT) at 37 °C in a humidified atmosphere of 5 % CO₂. Dorsal root ganglion (DRG) neurons were freshly isolated and provided by Dr. Zhuan Zhou's lab (Institute of Molecular Medicine, Peking University). Briefly, adult Wistar rats (male, ~60 g) were euthanized by an intraperitoneal injection of 0.6 ml chloral hydrate solution (10 %). Dorsal root ganglions were isolated in ice-cold DMEM (low glucose, Gibco) bubbled with 5 % CO₂/95 % O₂. The tissues were treated with trypsin (0.3 mg/mL) and collagenase (1 mg/mL) for 30 min at 37 °C. Then, the cells were dissociated with a pipette and plated on a poly-lysine (Sigma)-coated cell-culture dish. The cells were maintained in MEM-F12 (Gibco) supplemented with 10 % fetal bovine serum (Gibco) and were used within 2–8 h after plating. Only the small (15–25 μm, C-type) neurons without apparent processes were used. Inevitably, some neurogliaocytes were co-isolated during the preparation process, leading to both DRG neurons and neurogliaocytes being co-cultured in the plate and further used for siRNA transfection. Primary vascular smooth muscle cells (VSMCs) from the thoracic aorta of SD rats (180–200 g) were provided by Dr. Rui-Ping Xiao's lab (Institute of Molecular Medicine, Peking University). Here, the rats were sacrificed with an overdose of pentobarbital sodium (100 mg/kg) by intraperitoneal injection before the aorta was excised. The VSMCs were cultured in DMEM with 10 % fetal bovine serum (FBS, Invitrogen).

Fluorescence-activated cell sorting (FACS)

MDA-MB-231 cells were plated in 12-well plates (1×10^5 per well) one day before transfection

and being cultured in L15 medium supplemented with 10 % FBS, 100 U/ml penicillin and 100 mg/ml streptomycin to 60–70 % confluence. After replacing L15 with Opti-MEM, a reduced serum medium, complexes containing 100 pmol FAM-labeled siRNA were added into each well. After incubation at 37 °C for 4 h, 2 ml of fresh L15 containing 10 % FBS was added, followed by further incubation for 4 h. Then, the cells were washed three times with 1 ml of ice-cold 1×PBS to remove residual free complexes and siRNAs, subsequently suspended in 400 µl of ice-cold 1×PBS and introduced into a FACS Calibur flow cytometer (Becton Dickinson, San Jose, CA, USA).

Subcellular localization

MDA-MB-231 cells were plated in 6-well plates (2×10^5 per well) with glass coverslips (one coverslip per well) at the bottom one day before transfection. NGR-10R/siRNA complexes containing 150 pmol (7.5 µl, 20 µM) FAM-labeled siRNA were transfected into cells according to the above-mentioned protocol. A Zeiss confocal microscope (LSM510, Carl Zeiss, Germany) was used to record the subcellular distribution of the siRNA ~10 h post transfection. LysoTracker Red DND-99 (Invitrogen, Carlsbad, CA) was used to indicate the endosomes and lysosomes before imaging.

MTT assay

An MTT assay was employed to evaluate the cytotoxicity of the peptide/siRNA complexes. MDA-MB-231 cells were seeded at 10000 cells per 100 µl of L15 per well on a 96-well plate

and allowed to adhere overnight at 37 °C. For the test panel A (supplementary figure S6a), the cells were transfected with complexes containing 6.25 pmol (means 50 nM for the transfection concentration) siRNA in 25 µl of Opti-MEM. For the test panel B (supplementary figure S6b), the transfection concentrations of siRNA ranged from 1600 nM to 25 nM. Blank NGR-10R without siRNA loading, 'NGR-10R/siRNA 200:0', served as a control by adding equal moles of peptide with 'NGR-10R/siRNA 200:1'. Four hours later, 200 µl of fresh complete L15 medium was added. After an additional 20 h of culture in the presence of 10 % FBS, 200 µl of the medium was removed, and 2 µl of MTT was added into each well, followed by another 4 h of incubation under the same incubator conditions. Then, all the medium was removed, and 50 µl DMSO was added and incubated for 30 min at 37 °C to dissolve formazan. Finally, the absorbance was read at 540 nm with a reference wavelength of 650 nm, and the absolute absorbance (OD_{net540}) was OD_{540} minus OD_{650} . To compare the relative viability, all the data were presented as the mean percentage \pm S.D. in two replicate samples compared with the absorbance value of mock-treated cells. The cell viability was calculated as

$$\text{Cell viability (\%)} = (OD_{net540(\text{sample})}/OD_{net540(\text{mock})}) \times 100,$$

where $OD_{net540(\text{sample})}$ is the absorbance at 540 nm of the transfected cells and $OD_{net540(\text{control})}$ is the absorbance at 540 nm of the mock control (nontransfected cells).

Real-time PCR

To assess whether siLamin A/C (against LMNA gene) transfected by NGR-10R could

suppress the expression of a targeted gene, real-time quantitative PCR was performed. MDA-MB-1231 cells were plated in 12-well plates (1×10^5 per well) one day before transfection and incubated in L15 to approximately 60 % confluence. Then, the medium was removed and replaced with 1 ml of Opti-MEM. Subsequently, 200 μ l of complexes containing 100 pmol siLamin A/C were added into each well (the final transfection concentration of siRNA was approximately 80 nM). Here, lipofectamine 2000 was a positive control, and each sample was tested in two replicate wells. After 4 h of incubation, 2 ml of fresh L15 containing 10 % FBS was added, and the cells were further incubated for 20 h. The total RNA of the cells was extracted with Trizol according to the manufacturer's protocol. Cells from the two replicates were mixed before RNA extraction. Then, cDNA was prepared by two-step reverse transcription. First, 2 μ g total RNA, 1 μ l of oligo dT and ddH₂O (5 μ l in total) was mixed and incubated for 5 min at 70 °C, followed by immediately transferring onto ice. Then 5.5 μ l of RNase-free water, 4 μ l of 5 \times reaction buffer, 2.5 μ l of MgCl₂ (500 mM), 1 μ l of dNTP (10 mM), 1 μ l of RNase inhibitor, and 1 μ l of reverse-transcription enzyme were added into the precooled tube, followed by a reaction at 25 °C for 5 min, 42 °C for 1 h and 75 °C for 15 min, respectively. A real-time PCR reaction system (0.1 μ l of Tag enzyme, 0.5 μ l of dNTP (10 mM), 2.5 μ l of 10 \times reaction buffer, 1 μ l of Sybr Green, 0.75 μ l of MgCl₂ (500 mM), 18.15 μ l of RNase-free water, 1 μ l of cDNA, and 1 μ l of primer mixture (20 μ M)) was prepared and first hot-started for 5 min at 95 °C before 40 cycles of 30 s at 95 °C, 30 s at 55 °C and 30 s at 72 °C. After the melting procedure was completed, the samples were stored at 4 °C. The expression level of Lamin A/C was analyzed by the Ct (cycle threshold) values using standard protocol.

Western blotting

MDA-MB-231 cells or HUVECs were seeded in 6-well plates (2×10^5 per well). siRNA transfection was then performed using complexes containing 100 pmol siLamin A/C. After incubation for 48 h, the total protein was extracted using the standard protocol. The protein-extracted lysate was resuspended in 75 μ l of protein lysis buffer containing 1 μ l of proteinase inhibitor cocktail. Western blotting was conducted using a wet system at a loading of 20 μ g protein. The blots were incubated overnight at 4 °C with the monoclonal antibody diluted to 1:1000 (for lamin A/C) or 1:5000 (for GAPDH), followed by incubation with HRP-conjugated goat anti-rabbit (for lamin A/C) or anti-mouse (for GAPDH) secondary antibodies (1:5000) at room temperature for 2 h. Finally, the membranes were exposed using Bio-Rad Universal Hood II (Bio-Rad, Bossier City, LA).

Animals

Male C57BL/6 mice (for *in vivo* distribution assay, weighing 18–22 g) and female BALB/c nude mice (for tumor-targeting evaluation, weighing 18–22 g) were purchased from the Academy of Military Medical Sciences of China. The animals were maintained in Peking University Laboratory Animal Center (an AAALAC-accredited and specific-pathogen-free (SPF) experimental animal facility). All the procedures involving experimental animals were performed in accordance with protocols approved by the Institutional Animal Care and Use Committee (IACUC) of Peking University.

Biodistribution of complexes in C57BL/6

To characterize the biodistribution profile of the NGR-10R/siRNA complexes, male C57BL/6 mice 5–7 weeks old, weighing 18–22 g, were used to perform *in vivo* imaging. Typically, the hair color of C57BL/6 mice is black. It is well known that black material absorbs the most light, including visible and infrared light, which may result in attenuation of fluorescence signal. Moreover, the color of the mouse skin changes with the hair cycles, anagen (active growth, black), catagen (controlled regression through apoptosis, gray), and telogen (resting phase, pink). Our previous studies also observed that the black skin will also cause signal attenuation significantly. Hence, the mice with black skin were excluded in these assays, and the abdomen of C57BL/6 mice was pre-shaved one day before administration to facilitate observation. In addition, siRNAs used for *in vivo* imaging were labeled with Cy5. Cy5 is fluorescent in the red region (excitation at 650 nm, emission at 670 nm), exhibiting much stronger tissue penetration capability than the fluorophores fluorescent in the green region (such as EGFP, FAM, *etc.*). A given formulation was administered to each mouse *via* tail vein injection at a dose of 2.5 mg/kg (for siRNA). The Cy5 fluorescence signal of the whole body was examined using a Kodak *in vivo* imaging system (Kodak In-Vivo Imaging System FX Pro, Carestream Health, USA) at given time points. The mice were anesthetized with a gas mixture of oxygen and isoflurane using Matrix VIP3000 isoflurane vaporizer (Matrix, USA) during imaging. At the end-point, the mice were sacrificed by cervical dislocation, and the major organs were isolated and re-examined. The above experiments were replicated three times independently. Quantitative analyses were performed using a molecular imaging

software package (Carestream Health, USA).

***In vivo* tumor-targeting properties of NGR-10R/siRNA complexes**

To validate the tumor-targeting properties of the NGR-10R/siRNA complexes, 5×10^6 MDA-MB-231 cells were subcutaneously injected into the right axillary fossa of female BALB/C nude mice. When the tumor had grown to approximately 400 mm^3 , the indicated formulation was given to each mouse by intravenous injection. The mice were anesthetized by intraperitoneal (i.p.) injection of pentobarbital sodium (50 mg/kg), and images were taken at the indicated time points using a Kodak *in vivo* imaging system. Twenty-four hours later, the mice were sacrificed by cervical dislocation, and the major tissues including tumors were isolated and re-examined. Then, the tumors were placed in Omnisette tissue cassettes, embedded in OCT, frozen in a pre-chilled Dewar flask containing liquid nitrogen/dry ice slurry for ~1 min until the OCT turned white and opaque. Subsequently, the specimens were cut into 10- μm sections on a cryostat. The sections were stained by DAPI to visualize the nucleus and FITC-labeled Phalloidin to visualize the F actin. The rough cell outline was displayed by F actin. Finally, the cryosections were observed by confocal microscope (LSM510, Carl Zeiss, Germany).

Statistical analysis

The data were expressed as the mean \pm SD or mean \pm SEM, which was indicated in figure legends. The statistical variance was calculated by a *t*-test; $P < 0.05$ was considered

statistically significant.

Results and discussion

siRNA binding capacity

To evaluate the siRNA binding capacity of NGR-10R peptide, gel retardation assays were performed with a serum-stable siRNA, si-NC67-M. Using this siRNA excluded possible siRNA degradation in a gel shifting assay. NGR-10R/siRNA complexes were self-assembled by directly mixing peptide and siRNA solutions and incubating them for 15–20 min at room temperature (Scheme 1a). The gel shift results indicated that siRNAs were entrapped well by the peptides at molar ratios of NGR-10R and siRNA higher than 25:1 (Fig. 1a). Lesser siRNAs could run out from the gel wells with an increased molar ratio. A similar pattern was observed when a FAM-labeled NC siRNA was used (Fig. 1b). Moreover, the NGR-10R/siRNA complexes were stable not only in DEPC water but also in Opti-MEM, an optimized cell culture medium used for nucleic acid transfection (Fig. 1c). In addition, polyarginine 10R, without the NGR motif at the N terminal of the peptide, exhibited relatively weaker siRNA binding capacity compared with NGR-10R, as more siRNAs run into the gel at the same molar ratios (Fig. 1a). This finding might be attributed to its short peptide length, which exhibits poorer siRNA entrapping capability compared with the long counterpart.

RNase resistance

An RNase resistance assay was performed to investigate whether the peptide's binding could protect siRNAs from attack by RNase and therefore enhance their stability.

Double-stranded small RNA, mmu-miR-672, was used in this assay. Both naked RNA and peptide/RNA complexes were exposed in 20 % native PAGE. It was demonstrated that free mmu-miR-672 was degraded rapidly in fetal bovine serum (FBS) (Fig. 1d, left panel). In contrast, after being encapsulated by NGR-10R, this RNA was stable in serum for more than 12 h (Fig. 1d, right panel). The protection effects were likely due to the compact nanostructures formed by the peptide, and siRNA provided steric hindrance. Moreover, in accordance with the gel retardation data (Fig. 1a-c), peptide/siRNA complexes without digesting by proteinase K could not run out from the gel well (Fig. 1d, right panel, untreated complexes).

Characterization of physical-chemical properties of peptide/siRNA complexes

Transmission electron microscope (TEM) and dynamic light scattering (DLS) were used to characterize the morphology, size, polydispersity index (PDI) and zeta potential of NGR-10R/siRNA complexes at molar ratios of 20:1, 50:1 and 100:1. TEM data revealed that the complexation of peptide and siRNA formed regularly spherical nanostructures, with sizes ranging from a few tens of nanometers to two hundreds of nanometers (Fig. 2a, Table 1). A DLS assay revealed that the Z-average particle size calculated based on intensity was approximately 200 nm for all three complexes, whereas the size of RVG-9dR/siRNA complexes with molar ratios of 20:1 and 50:1 were 97 nm and 67 nm, respectively (Fig. 2b, Table 1). RVG-9R is a well-defined peptide that can effectively mediated siRNA delivery into central nervous system and macrophages by specifically binding to the acetylcholine receptor (AChR) expressed on the targeting cells^{51, 52}. It is a fusion peptide consisting of 41

amino acids and contains an RVG motif derived from rabies virus glycoprotein and nona-D-arginine residues (9dR). In accordance with NGR-10R, RVG-9dR also possesses one targeting moiety in each peptide molecule. RVG-9dR/siRNA exhibited a smaller particle size compared with NGR-10R/siRNA. Except for the polyarginine (9dR or 10R) at the C-terminal, RVG-9dR possesses a much longer N-terminal amino acid (aa) sequence (32 aa) compared with NGR-10R (6aa), which might result in stronger siRNA entrapping capacity and consequently the formation of smaller particles. This finding was further supported by the fact that 10R manifested a poorer siRNA loading capability compared with NGR-10R (Fig. 1a). Here, 10R could be considered to be the peptide with zero amino acid (0 aa) at the N-terminal. Thus, (i) the particle diameter (d) measured by DLS could be calculated based on the intensity (Z-average), volume or number. Because the larger particles contributed more than the smaller ones according to the equation for the intensity or volume-based analysis, the size relationship of the three models usually was as follows: d (intensity) $>$ d (volume) $>$ d (number)^{53, 54}. Therefore, the sizes of most of the NGR-10R/siRNA particles actually were smaller than 200 nm. In addition, (ii) the size measured by DLS was the hydrodynamic diameter, which is usually slightly larger than the actual physical size^{55, 56}. (iii) This size range (approximately 200 nm) still met the requirement of enhanced permeability and retention (EPR) effect that facilitated nanoparticles accumulating into tumor tissue⁵⁷. (iv) In addition to the passive targeting mechanism benefitting from the proper size distribution, the active targeting moiety, the NGR motif, would further assist nanoparticles being entrapped by tumor tissue. Therefore, the size distribution patterns of NGR-10R/siRNA with molar ratios of 20:1, 50:1 and 100:1 were acceptable for further *in vitro* and *in vivo*

applications. The PDI of NGR-10R/siRNA complexes with molar ratios of 20:1, 50:1 and 100:1 were 0.225, 0.284 and 0.296, respectively (Table 1). Moreover, the size and PDI of lipofectamine 2000/siRNA complexes were 140.5 nm and 0.261, respectively (Table 1)⁵⁸. Lipofectamine 2000 (Invitrogen) is a commercial reagent popularly used for *in vitro* nucleic acids transfection.

In addition, the zeta potentials of these three NGR-10R/siRNA formulations were 10–30 mV. The lipofectamine 2000/siRNA and RVG-9dR/siRNA complexes displayed zeta potentials of 24.40 mV and 4–7 mV, respectively (Table 1)⁵⁸. Naked siRNA, in line with expectation, exhibited a negative charge (-8.38 mV) in diethylpyrocarbonate (DEPC) water (Table 1)⁵⁸.

NGR-10R-mediated siRNA transfection *in vitro*

CD13 (aminopeptidase N) was identified as the specific receptor of the NGR motif⁴². Meanwhile, the cyclic *iso*DGR motif could be generated from the cyclic NGR motif through a non-enzymatic and spontaneous isomerization process⁴². Thus, integrin $\alpha_v\beta_3$ and/or $\alpha_v\beta_5$ would be recruited as the receptor(s) of the *iso*DGR motif under this circumstance. As a result, both the CD13 and integrin subfamily would theoretically be the specific receptors under different conditions when the NGR motif was employed as the targeting ligand for drug delivery.

MDA-MB-231 is a breast cancer cell line that lowly expresses CD13^{45, 59, 60} and highly expresses $\alpha_v\beta_3$ (CD13⁻/ $\alpha_v\beta_3$ ⁺)⁶¹⁻⁶³. Because it is not uncommon that receptor expression levels and profiles vary lab to lab for seemingly identical cell lines, PCR assay was performed to confirm that the MDA-MB-231 cell used in this study do indeed show the

reported CD13/integrin expression profile. From supplementary figure. S2, we observed clear PCR products with right length for GAPDH and ITGAV (integrin α_v). The product of ITGAV exhibited comparable grayscale with GAPDH product (a control in this assay), suggesting a high expression level of integrin α_v in MDA-MB-231. By contrast, it was failed to obtain PCR product for CD13. Therefore, to explore the feasibility of siRNA delivery mediated by a NGR motif-containing peptide in the CD13⁻/ $\alpha_v\beta_3$ ⁺ cell line, MDA-MB-231 was used in this study.

Fluorescence-activated cell sorting (FACS) and FAM-labeled siRNA were applied to investigate NGR-10R-mediated siRNA internalization. Data indicated that peptide/siRNA complexes were taken up efficiently by MDA-MB-231. Both the ratio of fluorescence-positive cells (representing cells that have internalized siRNAs) and the mean fluorescence intensity (MFI) (representing the amount of siRNAs entering cells) increased upon increasing the molar ratio of peptide and siRNA. The MFI of cells treated with NGR-10R/siRNA at the molar ratio of 200:1 was comparable with that of lipofectamine 2000-transfected cells (Fig. 3). Lipofectamine 2000 is a widely used reagent that is considered to be the gold standard for *in vitro* nuclei acid transfection. Moreover, although RVG-9dR enabled efficient siRNA delivery to the central nervous system⁵¹ and macrophages⁵², it could not deliver siRNA into MDA-MB-231 (Fig. 3b). The receptor of RVG-9dR is AchR⁵¹. In total, 17 subunits of AchR have been identified to date, among which $\alpha 7$ is the main interaction unit^{51,64}. In addition, it was reported that only $\alpha 5$, $\alpha 9$ and $\alpha 10$ subunits were expressed by MDA-MB-231, and $\alpha 1$, $\alpha 2$, $\alpha 3$, $\alpha 4$, $\alpha 6$, $\alpha 7$, $\beta 2$, $\beta 3$ and $\beta 4$ were not detected in MDA-MB-231⁶⁵. This finding explained why siRNAs could not be delivered into MDA-MB-231 cells in an AchR-mediated

endocytosis manner. It also suggested that only nanostructure itself, even with an ideal size distribution profile (Table 1), was insufficient to trigger effective internalization for such kind of single-component and peptide-based delivery system.

Because CD13 was lowly expressed by MDA-MB-231, together with the fact that RVG-9dR failed to transfect siRNA into MDA-MB-231, NGR-10R mediated efficient siRNA internalization should be attributed to the cyclic *iso*DGR motif yielded from the cyclic NGR motif. MDA-MB-231 highly expressed integrin $\alpha_v\beta_3$ and $\alpha_v\beta_5$, the specific receptor of *iso*DGR. It was well known that the cyclic NGR or *iso*DGR motif exhibited much higher binding affinity with its receptor compared with their corresponding linear one^{14, 42}. It was also reported that the cyclic *iso*DGR motif even exhibited a higher binding affinity than the cyclic RGD (Arg-Gly-Asp) motif⁴⁰, a well-known integrin ($\alpha_v\beta_3$)-recognizing tripeptide. The peptide of CNGRCG used in this study exhibits a rapid isomerization process with a half-life of several hours (2-4 h)³⁹. Hence, siRNAs might enter MDA-MB-231 cells *via iso*DGR-mediated endocytosis (Scheme 1b).

In addition, the RGD10-10R/siRNA complexes consisting of siRNA and RGD10-10R, a cyclic RGD motif-containing polypeptide, exhibited relative higher siRNA transfection efficiency than NGR-10R/siRNA complexes at the same molar ratios when the molar ratios were lower than 100:1⁵⁸. However, RGD10-10R/siRNA and NGR-10R/siRNA displayed similar internalization patterns when the molar ratios increased to 200:1⁵⁸. These results might be due to insufficient NGR peptides transforming into *iso*DGR peptides when the molar ratios were relatively low; however, adequate *iso*DGR peptides were generated when more NGR peptides were applied. Furthermore, Ruoslahti E. and colleagues⁷ demonstrated the

successful use of the NGR peptide for cancer therapy, where the MDA-MB-231 cell was employed. Together with the fact that RVG-9dR failed to transfect siRNA into the cells, we believed that a proportion of NGR-10R peptides were spontaneously transformed into *iso*DGR, triggering efficient siRNA transfection in MDA-MB-231.

Subcellular localization of NGR-10R/siRNA complexes

A confocal microscope was used to investigate the subcellular localization of peptide/siRNA complexes. LysoTracker red, a pH-sensitive dye that could freely penetrate the cell membrane, was applied to indicate endosomes and lysosomes. The data illustrated that both granule-shaped and dispersive fluorescence signals (representing FAM-labeled siRNAs) were observed for both NGR-10R/siRNA and lipofectamine 2000/siRNA complexes, which are highlighted in the two enlarged fields (Fig. 4). Dispersively distributed siRNAs were considered to be the real active molecules that triggered RNAi. In contrast, naked siRNA and 10R/siRNA complexes showed faint fluorescence signals around the cell membrane, which most likely resulted from non-specific binding between FAM-labeled siRNA and certain molecules (such as glycoprotein) on the surface of the cell membrane (Fig. 4). Although several papers reported that polyarginine was a type of cell penetration peptide (CPP)^{66, 67}, 10R/siRNA complexes exhibited no transfection in this study. This finding might be due to a potential blocking effect existing between the complexes and cell membrane when 10R/siRNA complexes formed.

Unlike MDA-MB-231 cells, few or no peptide/siRNA complexes were internalized by primary rat dorsal root ganglia (DRG) neurons (the cells consist of dendrite, soma and axon, the

relatively larger cells in supplementary Fig. S3a), neurogliocytes (the smaller cells in supplementary Fig. S3a) and primary vascular smooth muscle cells (VSMCs) (supplementary Fig. S3b) for NGR-10R/siRNA complexes with a molar ratio of 100:1, which should be attributed to these cells negatively expressing both CD13 and integrin $\alpha_v\beta_3$. However, lipofectamine 2000/siRNA exhibited limited siRNA transfection into these cells, hinting that a non-specific interaction between the lipid of lipofectamine 2000 and cell membrane was involved.

***In vitro* gene silencing**

Real-time quantitative PCR (RT-qPCR) and Western blotting were applied to assess the *in vitro* gene silencing of NGR-10R/siRNA complexes. Anti-Lamin A/C siRNA was used in this study. Lamin A/C, also known as LMNA, is a component of the nuclear membrane structure that is encoded by the LMNA gene in humans⁶⁸. Lamin proteins are thought to be involved in nuclear stability, chromatin structure and gene expression. During apoptosis, Lamin A/C is specifically cleaved into a large (40-45kD) and small (28kD) fragment. The cleavage of lamins results in nuclear disregulation and cell death⁶⁹. Mutations in the LMNA gene are associated with several diseases, including Emery-Dreifuss muscular dystrophy, familial partial lipodystrophy, limb girdle muscular dystrophy, dilated cardiomyopathy, Charcot-Marie-Tooth disease, restrictive dermopathy and Hutchinson-Gilford progeria syndrome. A truncated version of lamin A, commonly known as progerin, causes Hutchinson-Gilford progeria syndrome^{70, 71}. Both the RT-qPCR and Western blotting data, collected from MDA-MB-231, indicated that over 30 % knockdown efficiency was achieved

for the NGR-10R/siRNA complexes with a high molar ratio of 200:1 (Fig. 5a, b). In addition, human umbilical vein endothelial cell (HUVEC), a cell that simultaneously expressed CD13⁶⁰ and $\alpha_v\beta_3$ ⁷² (CD13⁺/ $\alpha_v\beta_3$ ⁺), was employed to further evaluate the *in vitro* transfection efficiency. The Western blotting data indicated that approximately 30 % repression of Lamin A/C's expression was also observed for the NGR-10R/siRNA complexes with a molar ratio of 20:1, suggesting a higher silencing efficiency compared with two commercial transfection reagents, lipofetamine 2000 and X-TremeGENE (Fig. 5c). Because HUVEC is known to be difficult to transfect, such a knockdown efficiency was satisfactory. However, for MDA-MB-231, the significant peptide/siRNA internalization observed by the FACS and confocal analyses did not result in remarkable gene silencing, which might be attributed to their relative weak capability of escaping from the endosome/lysosome. Furthermore, it was also possible that peptide/siRNA complexes successfully escaped from the endosome/lysosome but that the siRNAs were not subsequently released from the complexes and therefore failed to trigger RNAi. This speculation was supported by the phenomena that siRNAs were entrapped tightly by the peptide (Fig. 1a) and that a large portion of siRNAs were dispersively localized in the cell cytoplasm (Fig. 4).

***In vivo* biodistribution**

To explore the biodistribution profile of NGR-10R/siRNA complexes, *in vivo* fluorescent imaging was performed with 18–22 g male C57BL/6 mice and a serum-stable siRNA, NC siRNA. Naked Cy5-labeled NC siRNA or peptide/siRNA complexes were intravenously administered into the mice at a dose of 2.5 mg/kg (for siRNA). The fluorescence signal was

detected at the indicated time points by an *in vivo* imaging system (Kodak In-Vivo Imaging System FX Pro, Carestream Health, USA). The peptide/siRNA complexes with molar ratios of 50:1 and 20:1 displayed strong liver accumulation, whereas the naked siRNA exhibited a much weaker siRNA signal at the same time points post administration (Fig. 6). In addition, a large portion of siRNAs also accumulated in the submandibular gland, bulbourethral gland, pancreas, spleen and kidneys (Fig. 6). Based on their different structural properties of capillary, endothelial systems can be mainly divided into three classes: (i) continuous and nonfenestrated capillaries (e.g., the heart, lung, muscle and brain), (ii) continuous and fenestrated capillaries (e.g., the gastrointestinal tract, exocrine/endocrine glands and kidney glomerulus), and (iii) discontinuous and fenestrated endothelium (e.g., liver sinusoidal capillaries)⁷³. For the latter two kinds of endothelial systems, siRNAs themselves or complexes can penetrate blood vessels and reach corresponding tissues. Most of siRNAs will be excreted out from the body by accumulating into kidneys and bladder. In addition, siRNAs may be also processed in liver, secreted into the gallbladder, and eliminated out from the body along the intestine^{48, 74}. No significant difference was observed between naked-siRNA-treated mice and peptide/siRNA-complexes-treated mice for the submandibular gland, bulbourethral gland, pancreas and kidney, suggesting a tissue-structure-derived distribution profile.

Tumor-targeting properties of NGR-10R/siRNA complexes

An MDA-MB-231 xenografted murine model was used to explore the tumor-targeting properties of peptide/siRNA complexes. Tumor cells were injected subcutaneously into the

right axillary fossa of the BALB/C nude mice. When the tumors grew to approximately 400 mm³, the mice were given the indicated formulations, followed by fluorescent imaging at desired time points post administration. The data proved that all three complexes with molar ratios of 20:1, 50:1 and 100:1 accumulated in the tumor remarkably (Fig. 7a). Images acquired on isolated tissues after 24 h further confirmed that siRNAs were successfully delivered into tumors by NGR-10R (Fig. 7b, c). For clarification, the absolute MFIs in Fig. 6 and Fig. 7 are not comparable because these two assays were performed under different experimental conditions. In addition, cryosections were prepared and stained with FITC-labeled phalloidin (to indicate the rough cell outline, green) and DAPI (for highlighting the nuclei, blue). Confocal laser scanning microscope (CLSM) images demonstrated that obvious red siRNA signals were observed on the tumor cryosections for all three peptide/siRNA complexes with molar ratios of 20:1, 50:1 and 100:1. More importantly, siRNAs were mainly distributed in the cell cytoplasm where RNAi occurred, especially for the complexes with a molar ratio of 20:1 (Fig. 7d). In accordance with the imaging data collected in normal C57BL/6 mice, peptide/siRNA complexes also accumulated in submandibular gland and kidneys remarkably in the xenografted murine model (Fig. 7, supplementary Fig. S4 and S5).

In an additional test for tumor-targeted delivery of siRNA, naked siRNA was included, and blank NGR-10R was applied to compete with NGR-10R/siRNA complex for their receptor binding (data not shown). Blank NGR-10R was given into the mice one hour before the administration of NGR-10R/siRNA formulation. It was observed that the binding of NGR-10R to siRNA significantly reduced the excitation/emission efficiency of Cy5 fluorophore

compared to naked siRNA. Pre-injected NGR-10R did reduce the accumulation of NGR-10R/siRNA complexes in tumor tissues, which demonstrated the NGR motif played a pivotal role in tumor-targeted transportation of siRNA *in vivo*.

Three pivotal issues might facilitate siRNAs being transported into tumor cells. First, both CD13⁸ and integrin $\alpha_v\beta_3$ ^{75, 76} were highly expressed in the endothelium cells of the neovasculature. Consequently, both NGR-10R/siRNA complexes and their isomerization products, *iso*DGR/siRNA complexes, could recognize the neovasculature by binding to CD13 and $\alpha_v\beta_3$, respectively (Scheme 1c). In this manner, siRNAs could be delivered into the endothelial cells of the neovasculature and trigger RNAi there. Alternatively, it was possible that partial complexes that failed to escape from endosomes and lysosomes would be released from the endothelial cells, assisting them to finally attach tumor cells (Scheme 1c). Second, the particle size of the complexes was approximately 200 nm, which met the requirement of an enhanced permeability and retention (EPR) effect that facilitated particles accumulating into tumor tissue⁵⁷. Thus, siRNAs could be transported into the tumor by NGR-10R (Scheme 1c). Third, peptide/siRNA complexes could enter the cell through *iso*DGR/ $\alpha_v\beta_3$ -derived endocytosis (Scheme 1b).

Furthermore, it was demonstrated that well siRNA transportation was achieved in the MDA-MB-231 (CD13⁻/ $\alpha_v\beta_3$ ⁺) xenografted tumor model. The delivery efficiency may be further enhanced if another tumor cell line that simultaneously expresses CD13 and $\alpha_v\beta_3$ (CD13⁺/ $\alpha_v\beta_3$ ⁺) is tested. In summary, NGR-10R constitutes an ideal tumor-targeting vector that can be used for siRNA delivery.

Toxicity evaluation *in vitro* and *in vivo*

An MTT assay was used to evaluate the biocompatibility of the NGR-10R/siRNA complexes. The cell viability data (supplementary Fig. S6) collected in MDA-MB-231 indicated that NGR-10R/siRNA complexes with various molar ratios displayed ideal biocompatibility. The cell viability remained more than 80% compared to untreated cells even the transfection concentration has increased to 1600 nM. Blank NGR-10R peptide, 'NGR-10R/siRNA 200:0', also displayed well biocompatibility at a series of transfection concentrations, in which the peptide amounts transfected into the cell were the same with the formulation of 'NGR-10R/siRNA 200:1'. However, lipofectamine 2000 showed significant cytotoxicity at 1600 nM. X-TremeGENE exhibited a viability of 88 % compared with cells without any treatment (mock) even at a relative low transfection concentration (50 nM), suggesting its potential cytotoxicity to the cells.

In addition, *in vivo* safety was evaluated using normal CD-1 mice. Here, lipopolysaccharide (LPS) and PBS were included as positive and negative control, respectively. NGR-10R/siRNA complexes with the molar ratios of 20:1 and 50:1 were intravenously injected into the mice at the dose of 2.5 mg/kg (for siRNA). LPS was intraperitoneally injected into the mice at the dose of 5.0 mg/kg. Mice were sacrificed at 4, 24 and 72 hours post administration and subjected to evaluation of various safety indicators. The organ coefficients of liver and spleen were calculated, as shown in supplementary figure S7. It was proved that LPS significantly elevated the organ coefficients of mice, revealing its high toxicity to mice. However, both two NGR-10R/siRNA formulations showed no increase of organ coefficients. Furthermore, no influence on liver and renal function was observed for

peptide/siRNA complexes (supplementary Fig. S8). Triglyceride (TG) was greatly elevated for LPS-treated mice at 4 hours post injection (supplementary Fig. S8), suggesting abnormal lipid metabolism occurred during this time frame for these mice. More important, compared to 1×PBS-treated mice, peptide/siRNA-treated mice exhibited no significant change of cytokines (TNF-alpha, IFN-gamma and IL-6) at all three time points post administration (supplementary Fig. S9). By contrast, as all three cytokines were drastically elevated, remarkable immunostimulation was observed for LPS-treated mice at all three time points (supplementary Fig. S9). Collectively, NGR-10R showed ideal biocompatibility both *in vitro* and *in vivo*.

Conclusion

The lack of efficient, safe and clinically applicable delivery systems has severely hampered siRNA-based drug development. Cell penetration peptides are promising delivery reagents for siRNA delivery in clinical practice. In this study, the feasibility of the NGR-10R peptide was evaluated as a carrier to deliver siRNA into the CD13-negative cell line, MDA-MB-231. Physical-chemical characterization of peptide/siRNA complexes indicated that siRNAs were entrapped by peptides, forming spherical nanostructures that greatly enhanced the serum-resistance ability of the siRNA. FACS and confocal assays demonstrated that NGR-10R mediated efficient siRNA delivery into MDA-MB-231 cells and HUVEC, leading to potent gene silencing *in vitro*. However, no peptide/siRNA complexes were internalized by CD13 and $\alpha_v\beta_3$ dual-negative cells, such as DRG neurons, neurogliaocytes and VSMCs. Furthermore, *in vivo* fluorescent imaging revealed that siRNAs could be delivered into tumor tissue and localized in cell cytoplasm. For *in vitro* evaluation, *isoDGR*/ $\alpha_v\beta_3$ -mediated endocytosis contributed to the siRNA transfection (Scheme 1b), whereas for *in vivo* testing, both NGR/CD13 and *isoDGR*/ $\alpha_v\beta_3$ interaction assisted the tumor-targeted delivery (Scheme 1c). In conclusion, NGR-10R provides an ideal *in vitro* and *in vivo* siRNA delivery reagent, *isoDGR* motif may replace the current generation of integrin-binding molecules devoid of intrinsic paradoxical activation effects, and therefore both NGR and *isoDGR*-derived compounds can be used for siRNA drug development.

References

1. M. E. Davis, J. E. Zuckerman, C. H. Choi, D. Seligson, A. Tolcher, C. A. Alabi, Y. Yen, J. D. Heidel and A. Ribas, *Nature*, 2010, **464**, 1067-1070.
2. J. D. Heidel, Z. Yu, J. Y. Liu, S. M. Rele, Y. Liang, R. K. Zeidan, D. J. Kornbrust and M. E. Davis, *Proc Natl Acad Sci U S A*, 2007, **104**, 5715-5721.
3. J. Taberero, G. I. Shapiro, P. M. LoRusso, A. Cervantes, G. K. Schwartz, G. J. Weiss, L. Paz-Ares, D. C. Cho, J. R. Infante, M. Alsina, M. M. Gounder, R. Falzone, J. Harrop, A. C. White, I. Toudjarska, D. Bumcrot, R. E. Meyers, G. Hinkle, N. Svrzikapa, R. M. Hutabarat, V. A. Clausen, J. Cehelsky, S. V. Nochur, C. Gamba-Vitalo, A. K. Vaishnav, D. W. Sah, J. A. Gollob and H. A. Burris, 3rd, *Cancer Discov*, 2013, **3**, 406-417.
4. C. I. Wooddell, D. B. Rozema, M. Hossbach, M. John, H. L. Hamilton, Q. Chu, J. O. Hegge, J. J. Klein, D. H. Wakefield, C. E. Oropeza, J. Deckert, I. Roehl, K. Jahn-Hofmann, P. Hadwiger, H. P. Vornlocher, A. McLachlan and D. L. Lewis, *Mol Ther*, 2013, **21**, 973-985.
5. S. C. Wong, J. J. Klein, H. L. Hamilton, Q. Chu, C. L. Frey, V. S. Trubetskoy, J. Hegge, D. Wakefield, D. B. Rozema and D. L. Lewis, *Nucleic Acid Ther*, 2012, **22**, 380-390.
6. K. M. Wagstaff and D. A. Jans, *Curr Med Chem*, 2006, **13**, 1371-1387.
7. W. Arap, R. Pasqualini and E. Ruoslahti, *Science*, 1998, **279**, 377-380.
8. R. Pasqualini, E. Koivunen, R. Kain, J. Lahdenranta, M. Sakamoto, A. Stryhn, R. A. Ashmun, L. H. Shapiro, W. Arap and E. Ruoslahti, *Cancer Res*, 2000, **60**, 722-727.
9. F. Curnis, G. Arrigoni, A. Sacchi, L. Fischetti, W. Arap, R. Pasqualini and A. Corti, *Cancer Res*, 2002, **62**, 867-874.
10. A. Buehler, M. A. van Zandvoort, B. J. Stelt, T. M. Hackeng, B. H. Schrans-Stassen, A. Bennaghmouch, L. Hofstra, J. P. Cleutjens, A. Duijvestijn, M. B. Smeets, D. P. de Kleijn, M. J. Post and E. D. de Muinck, *Arterioscler Thromb Vasc Biol*, 2006, **26**, 2681-2687.
11. A. Corti, F. Curnis, W. Arap and R. Pasqualini, *Blood*, 2008, **112**, 2628-2635.
12. M. Oostendorp, K. Douma, T. M. Hackeng, A. Dirksen, M. J. Post, M. A. van Zandvoort and W. H. Backes, *Cancer Res*, 2008, **68**, 7676-7683.
13. F. Curnis, A. Sacchi, L. Borgna, F. Magni, A. Gasparri and A. Corti, *Nat Biotechnol*, 2000, **18**, 1185-1190.
14. G. Colombo, F. Curnis, G. M. De Mori, A. Gasparri, C. Longoni, A. Sacchi, R. Longhi and A. Corti, *J Biol Chem*, 2002, **277**, 47891-47897.
15. F. Curnis, A. Sacchi and A. Corti, *J Clin Invest*, 2002, **110**, 475-482.
16. N. Zarovni, L. Monaco and A. Corti, *Hum Gene Ther*, 2004, **15**, 373-382.
17. F. Curnis, A. Gasparri, A. Sacchi, A. Cattaneo, F. Magni and A. Corti, *Cancer Res*, 2005, **65**, 2906-2913.
18. A. Sacchi, A. Gasparri, F. Curnis, M. Bellone and A. Corti, *Cancer Res*, 2004, **64**, 7150-7155.
19. A. M. Gasparri, E. Jachetti, B. Colombo, A. Sacchi, F. Curnis, G. P. Rizzardi, C. Traversari, M. Bellone and A. Corti, *Mol Cancer Ther*, 2008, **7**, 3859-3866.
20. B. Zhang, B. Gao, S. Dong, Y. Zhang and Y. Wu, *Regul Toxicol Pharmacol*, 2011, **60**, 73-78.
21. R. Bieker, T. Kessler, C. Schwoppe, T. Padro, T. Persigehl, C. Bremer, J. Dreischaluck, A. Kolkmeier, W. Heindel, R. M. Mesters and W. E. Berdel, *Blood*, 2009, **113**, 5019-5027.
22. L. Liu, W. F. Anderson, R. W. Beart, E. M. Gordon and F. L. Hall, *J Virol*, 2000, **74**, 5320-5328.
23. F. Pastorino, C. Brignole, D. Marimpietri, M. Cilli, C. Gambini, D. Ribatti, R. Longhi, T. M. Allen, A. Corti and M. Ponzoni, *Cancer Res*, 2003, **63**, 7400-7409.
24. F. Pastorino, C. Brignole, D. Di Paolo, B. Nico, A. Pezzolo, D. Marimpietri, G. Pagnan, F. Piccardi, M. Cilli, R. Longhi, D. Ribatti, A. Corti, T. M. Allen and M. Ponzoni, *Cancer Res*, 2006, **66**, 10073-10082.
25. H. M. Ellerby, W. Arap, L. M. Ellerby, R. Kain, R. Andrusiak, G. D. Rio, S. Krajewski, C. R. Lombardo, R. Rao, E.

- Ruoslahti, D. E. Bredesen and R. Pasqualini, *Nat Med*, 1999, **5**, 1032-1038.
26. Y. Yokoyama and S. Ramakrishnan, *Cancer*, 2005, **104**, 321-331.
27. A. Dirksen, S. Langereis, B. F. de Waal, M. H. van Genderen, E. W. Meijer, Q. G. de Lussanet and T. M. Hackeng, *Org Lett*, 2004, **6**, 4857-4860.
28. M. G. Zauderer and L. M. Krug, *J Natl Compr Canc Netw*, 2012, **10**, 42-47.
29. V. Gregorc, P. A. Zucali, A. Santoro, G. L. Ceresoli, G. Citterio, T. M. De Pas, N. Zilembo, F. De Vincenzo, M. Simonelli, G. Rossoni, A. Spreafico, M. Grazia Vigano, F. Fontana, F. G. De Braud, E. Bajetta, F. Caligaris-Cappio, P. Bruzzi, A. Lambiase and C. Bordignon, *J Clin Oncol*, 2010, **28**, 2604-2611.
30. P. A. Zucali, M. Simonelli, F. De Vincenzo, E. Lorenzi, M. Perrino, M. Bertossi, R. Finotto, S. Naimo, L. Balzarini, C. Bonifacio, I. Timofeeva, G. Rossoni, G. Mazzola, A. Lambiase, C. Bordignon and A. Santoro, *Br J Cancer*, 2013, **108**, 58-63.
31. D. Lorusso, G. Scambia, G. Amadio, A. di Legge, A. Pietragalla, R. De Vincenzo, V. Masciullo, M. Di Stefano, G. Mangili, G. Citterio, M. Mantori, A. Lambiase and C. Bordignon, *Br J Cancer*, 2012, **107**, 37-42.
32. V. Gregorc, F. G. De Braud, T. M. De Pas, R. Scalamogna, G. Citterio, A. Milani, S. Boselli, C. Catania, G. Donadoni, G. Rossoni, D. Ghio, G. Spitaleri, C. Ammannati, S. Colombi, F. Caligaris-Cappio, A. Lambiase and C. Bordignon, *Clin Cancer Res*, 2011, **17**, 1964-1972.
33. A. Santoro, L. Rimassa, A. F. Sobrero, G. Citterio, F. Sclafani, C. Carnaghi, A. Pessino, F. Caprioni, V. Andretta, M. C. Tronconi, G. Finocchiaro, G. Rossoni, A. Zanoni, C. Miggiano, G. P. Rizzardi, C. Traversari, F. Caligaris-Cappio, A. Lambiase and C. Bordignon, *Eur J Cancer*, 2010, **46**, 2746-2752.
34. H. W. van Laarhoven, W. Fiedler, I. M. Desar, J. J. van Asten, S. Marreaud, D. Lacombe, A. S. Govaerts, J. Bogaerts, P. Lasch, J. N. Timmer-Bonte, A. Lambiase, C. Bordignon, C. J. Punt, A. Heerschap and C. M. van Herpen, *Clin Cancer Res*, 2010, **16**, 1315-1323.
35. T. Kessler, C. Schwoppe, R. Liersch, C. Schliemann, H. Hintelmann, R. Bieker, W. E. Berdel and R. M.esters, *Curr Drug Discov Technol*, 2008, **5**, 1-8.
36. M. Wickstrom, R. Larsson, P. Nygren and J. Gullbo, *Cancer Sci*, 2011, **102**, 501-508.
37. R. Tyler-Cross and V. Schirch, *J Biol Chem*, 1991, **266**, 22549-22556.
38. N. E. Robinson and A. B. Robinson, *Proc Natl Acad Sci U S A*, 2001, **98**, 944-949.
39. F. Curnis, R. Longhi, L. Crippa, A. Cattaneo, E. Dondossola, A. Bachi and A. Corti, *J Biol Chem*, 2006, **281**, 36466-36476.
40. A. Spitaleri, S. Mari, F. Curnis, C. Traversari, R. Longhi, C. Bordignon, A. Corti, G. P. Rizzardi and G. Musco, *J Biol Chem*, 2008, **283**, 19757-19768.
41. G. C. Alghisi and C. Ruegg, *Endothelium*, 2006, **13**, 113-135.
42. F. Curnis, A. Cattaneo, R. Longhi, A. Sacchi, A. M. Gasparri, F. Pastorino, P. Di Matteo, C. Traversari, A. Bachi, M. Ponzoni, G. P. Rizzardi and A. Corti, *J Biol Chem*, 2010, **285**, 9114-9123.
43. F. Curnis, A. Sacchi, A. Gasparri, R. Longhi, A. Bachi, C. Doglioni, C. Bordignon, C. Traversari, G. P. Rizzardi and A. Corti, *Cancer Res*, 2008, **68**, 7073-7082.
44. M. Ghitti, A. Spitaleri, B. Valentini, S. Mari, C. Asperti, C. Traversari, G. P. Rizzardi and G. Musco, *Angew Chem Int Ed Engl*, 2012, **51**, 7702-7705.
45. L. Hou, X. Zhao, P. Wang, Q. Ning, M. Meng and C. Liu, *PLoS One*, 2013, **8**, e53491.
46. L. Wang, J. Shi, H. Zhang, H. Li, Y. Gao, Z. Wang, H. Wang, L. Li, C. Zhang, C. Chen, Z. Zhang and Y. Zhang, *Biomaterials*, 2013, **34**, 262-274.
47. Y. Chen, J. J. Wu and L. Huang, *Mol Ther*, 2010, **18**, 828-834.
48. Y. Huang, J. Hong, S. Zheng, Y. Ding, S. Guo, H. Zhang, X. Zhang, Q. Du and Z. Liang, *Mol Ther*, 2011, **19**, 381-385.

49. J. Hong, Y. Huang, J. Li, F. Yi, J. Zheng, H. Huang, N. Wei, Y. Shan, M. An, H. Zhang, J. Ji, P. Zhang, Z. Xi, Q. Du and Z. Liang, *FASEB J*, 2010, **24**, 4844-4855.
50. C. D. Novina and P. A. Sharp, *Nature*, 2004, **430**, 161-164.
51. P. Kumar, H. Wu, J. L. McBride, K. E. Jung, M. H. Kim, B. L. Davidson, S. K. Lee, P. Shankar and N. Manjunath, *Nature*, 2007, **448**, 39-43.
52. S. S. Kim, C. Ye, P. Kumar, I. Chiu, S. Subramanya, H. Wu, P. Shankar and N. Manjunath, *Mol Ther*, 2010, **18**, 993-1001.
53. O. T. Mefford, M. R. J. Carroll, M. L. Vadala, J. D. Goff, R. Mejia-Ariza, M. Saunders, R. C. Woodward, T. G. St Pierre, R. M. Davis and J. S. Riffle, *Chem Mater*, 2008, **20**, 2184-2191.
54. D. Mahl, J. Diendorf, W. Meyer-Zaika and M. Epple, *Colloids and Surfaces A: Physicochem. Eng. Aspects*, 2011, **377**, 386-392.
55. S. I. Jenkins, M. R. Pickard, D. N. Furness, H. H. Yiu and D. M. Chari, *Nanomedicine (Lond)*, 2013, **8**, 951-968.
56. R. De Palma, S. Peeters, M. J. Van Bael, H. Van den Rul, K. Bonroy, W. Laureyn, J. Mullens, G. Borghs and G. Maes, *Chem Mater*, 2007, **19**, 1821-1831.
57. H. Maeda, J. Wu, T. Sawa, Y. Matsumura and K. Hori, *J Control Release*, 2000, **65**, 271-284.
58. Y. Huang, X. Wang, W. Huang, Q. Cheng, S. Zheng, S. Guo, H. Cao, X. J. Liang, Q. Du and Z. Liang, *Sci Rep*, 2015, **5**, 12458.
59. J. S. Shim, J. H. Kim, H. Y. Cho, Y. N. Yum, S. H. Kim, H. J. Park, B. S. Shim, S. H. Choi and H. J. Kwon, *Chem Biol*, 2003, **10**, 695-704.
60. R. Soudy, S. Ahmed and K. Kaur, *ACS Comb Sci*, 2012, **14**, 590-599.
61. S. Takayama, S. Ishii, T. Ikeda, S. Masamura, M. Doi and M. Kitajima, *Anticancer Res*, 2005, **25**, 79-83.
62. Y. Zhao, R. Bachelier, I. Treilleux, P. Pujuguet, O. Peyruchaud, R. Baron, P. Clement-Lacroix and P. Clezardin, *Cancer Res*, 2007, **67**, 5821-5830.
63. P. Wu, X. He, K. Wang, W. Tan, D. Ma, W. Yang and C. He, *J Nanosci Nanotechnol*, 2008, **8**, 2483-2487.
64. J. G. van den Boorn, M. Schlee, C. Coch and G. Hartmann, *Nat Biotechnol*, 2011, **29**, 325-326.
65. C. H. Lee, C. S. Huang, C. S. Chen, S. H. Tu, Y. J. Wang, Y. J. Chang, K. W. Tam, P. L. Wei, T. C. Cheng, J. S. Chu, L. C. Chen, C. H. Wu and Y. S. Ho, *J Natl Cancer Inst*, 2010, **102**, 1322-1335.
66. D. J. Mitchell, D. T. Kim, L. Steinman, C. G. Fathman and J. B. Rothbard, *J Pept Res*, 2000, **56**, 318-325.
67. S. M. Fuchs and R. T. Raines, *Biochemistry*, 2004, **43**, 2438-2444.
68. A. K. Kamat, M. Rocchi, D. I. Smith and O. J. Miller, *Somat Cell Mol Genet*, 1993, **19**, 203-208.
69. M. Goldberg, A. Harel and Y. Gruenbaum, *Crit Rev Eukaryot Gene Expr*, 1999, **9**, 285-293.
70. B. C. Capell and F. S. Collins, *Nat Rev Genet*, 2006, **7**, 940-952.
71. J. Rankin and S. Ellard, *Clin Genet*, 2006, **70**, 261-274.
72. G. C. Alghisi, L. Ponsonnet and C. Ruegg, *PLoS One*, 2009, **4**, e4449.
73. R. L. Kanasty, K. A. Whitehead, A. J. Vegas and D. G. Anderson, *Mol Ther*, 2012, **20**, 513-524.
74. D. J. Gary, H. Lee, R. Sharma, J. S. Lee, Y. Kim, Z. Y. Cui, D. Jia, V. D. Bowman, P. R. Chipman, L. Wan, Y. Zou, G. Mao, K. Park, B. S. Herbert, S. F. Konieczny and Y. Y. Won, *ACS Nano*, 2011, **5**, 3493-3505.
75. J. A. Varner and D. A. Cheresch, *Curr Opin Cell Biol*, 1996, **8**, 724-730.
76. W. Cai, S. S. Gambhir and X. Chen, *Methods Enzymol*, 2008, **445**, 141-176.

Acknowledgements

This work was supported by the Beijing Natural Science Foundation (5132015), National High-tech R&D Program of China (2014AA021103, 2012AA022501), National Drug Program of China (2011ZX09102-011-12, 2012ZX09102301-006), National Natural Science Foundation of China (81402863), Postdoctoral Science Foundation of China (2014M550008, 2015T80016) and the Natural Science Foundation of Jiangsu Province (BK2011381). We appreciate the technical support provided by Ms. Ning Hou (Institute of Molecular Medicine, Peking University) for the cryosection preparation. We are grateful to Dr. Xiaoli Tian, Dr. Zhuan Zhou and Dr. Rui-ping Xiao (all are from the Institute of Molecular Medicine, Peking University) for providing the HUVECs, DRG neurons/neurogliaocytes and VSMCs, respectively. The authors declare that there is no conflict of interest related to this paper.

Competing Financial Interests

The authors declare no competing financial interests.

Figure legends

Scheme 1. Fabrication of NGR-10R/siRNA complexes (a) and siRNA delivery processes *in vitro* (b) and *in vivo* (c). (a) By directly mixing NGR-10R peptide and siRNA at desired molar ratios and incubating them at room temperature for 15–20 min, NGR-10R/siRNA complexes were self-assembled. The NGR-10R/siRNA complexes can transform into *isoDGR-10R/siRNA* complexes because of a non-enzymatic and spontaneous deamidation reaction *via* which the asparagine of the cyclic NGR motif isomerizes into *iso*-aspartic acid (*isoAsp*, *isoD*). (b) siRNAs were transfected into MDA-MB-231 cells in a receptor ($\alpha_v\beta_3$)-mediated endocytosis (RME) manner *in vitro*. After being internalized by cells, the isomerization product *isoDGR-10R/siRNA* complexes escaped from the endosomes/lysosomes. Then, siRNAs were released from the complexes and loaded by RNA-induced silencing complex (RISC). Targeted message RNA complementary to the guide strand (antisense strand) of siRNA was selected and cleaved by agonaute protein. (c) After being administered into the animal by intravenous injection, peptide/siRNA complexes, including both NGR-10R/siRNA and *isoDGR-10R/siRNA* complexes, circulated in the animal body. Because the endothelial cells of the neovasculature in tumor tissue highly expressed both CD13 (the receptor of the NGR motif) and $\alpha_v\beta_3$ (the receptor of the *isoDGR* motif), peptide/siRNA complexes were entrapped by the tumor and accumulated there. Subsequently, two processes might have occurred. First, peptide/siRNA complexes directly permeated into the tumor tissue benefitting from the enhanced permeability and retention (EPR) effect. Therefore, *isoDGR/siRNA* complexes might enter the MDA-MB-231 cells *via* the same endocytosis pathway that *in vitro* siRNA transfection took (b). Second,

peptide/siRNA complexes could be internalized by endothelial cells *via* CD13 and/or $\alpha_v\beta_3$ mediated endocytosis. Consequently, the complexes could escape into the cytoplasm and induce gene silencing in endothelial cells. Alternatively, complexes that failed to escape from the endosome and lysosome also might excrete out from endothelial cells, enabling complexes to attach MDA-MB-231 tumor cells. Therefore, further RME and RNAi in tumor cells might occur in this way.

Fig. 1 Gel retardation (a-c) and RNase resistance (d) assays of NGR-10R/siRNA complexes. The siRNA loading capacity of NGR-10R was analyzed with two siRNAs, si-NC67-M (a, left panel) and FAM-labeled NC siRNA (b). Polyarginine (10R) was a control (a, right panel). Complexes incubated in Opti-MEM were also examined to assess the siRNA binding ability of peptide under this condition and the complexes stability (c). The RNase resistance was determined to validate the protection effect resulting from the peptide's binding using an unstable small RNA, mmu-miR-672. These data demonstrated that NGR-10R effectively bound small RNAs and significantly protected them from attack by RNase.

Fig. 2 TEM images (a) and particle size (b) of NGR-10R/siRNA complexes with various molar ratios.

Fig. 3 Internalization of complexes by MDA-MB-231 cell recorded by FACS. (a) FAM fluorescence intensity (represents the amount of complexes taken up by cells) and corresponding cell counts. RVG-9dR was included as a negative control because AchR, the

receptor of the RVG peptide, was barely expressed by MDA-MB-231. (b) Mean fluorescence intensity (MFI) and percentages of cellular uptake of complexes. The red and blue bars represent MFI and the percentage of uptake, respectively. Each bar represents the mean \pm SEM, n = 2.

Fig. 4 Intracellular localization of complexes recorded using confocal (LSM510, Carl Zeiss, Germany) laser scanning microscopy (CLSM). Images were acquired 8-10 h post transfection. LysoTracker red was used to stain F actin (red) to show the rough cell outline. siRNAs were labeled with FAM (green). The two bottom fields were enlarged from fields 1 and 2 indicated with white rectangles, respectively. The scale bars are indicated in the bright-field images.

Fig. 5 *In vitro* gene silencing evaluated by RT-PCR and Western blot. Relative mRNA (a) and protein (b) expression level of Lamin A/C in MDA-MB-231 cell. (c) Relative protein expression of Lamin A/C assessed in HUVEC, a cell highly expressing both CD13 and $\alpha_v\beta_3$. Commercial transfection reagents lipofectamine 2000 (Invitrogen) and X-TremeGENE (Roche) were included as controls. The numbers under the bands (b and c) represent the relative protein expression level. Each bar represents the mean \pm SD, n=3.

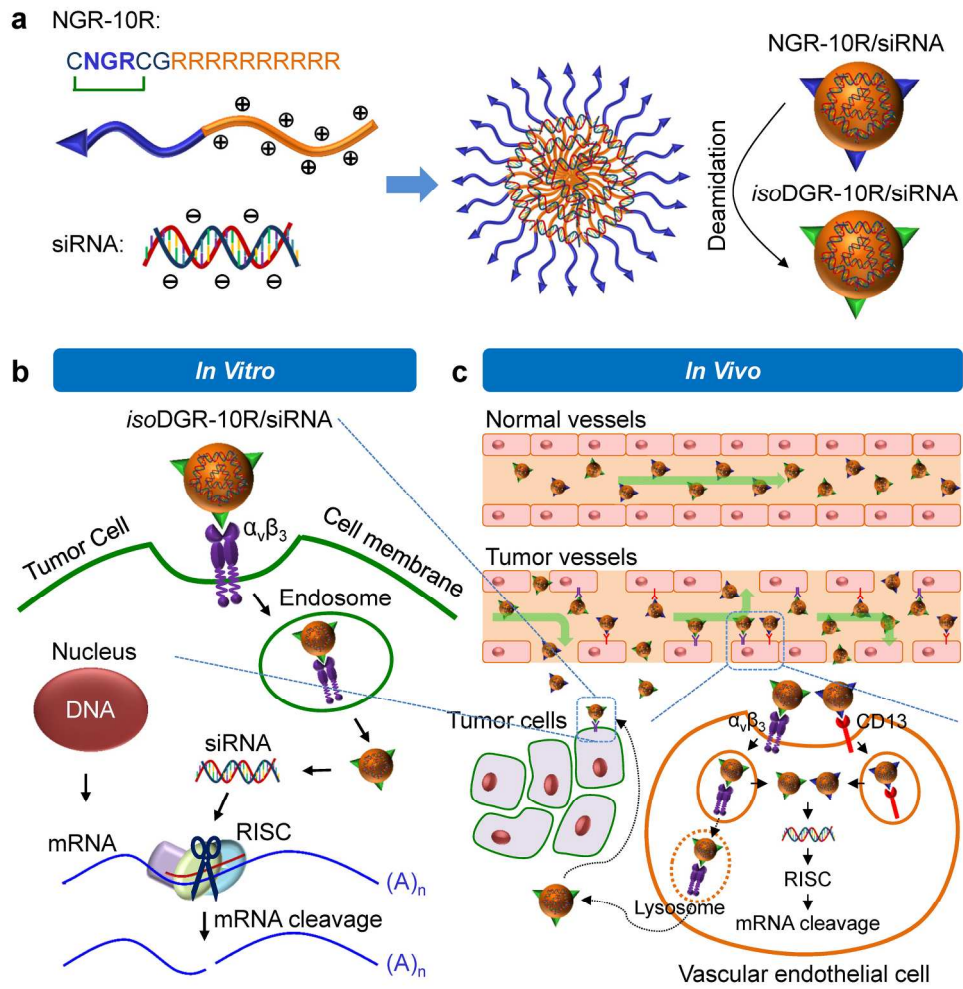
Fig. 6 *In vivo* distribution of complexes in C57BL/6 mice (2.5 mg/kg for siRNA). (a) Whole body imaging at given time points post intravenous administration. (b) Fluorescence detection of isolated organs of the mice at the end observation point. (c) Quantitative

analysis of (b) using a molecular imaging software package (Carestream Health, USA). The data were normalized to corresponding tissues from saline-treated animals. Each bar represents the mean \pm SEM of 2–3 independent experiments. * $P < 0.05$ and ** $P < 0.01$ vs. corresponding tissue(s) from naked siRNA treated mice. N = 3 for groups of saline, naked siRNA and 'NGR-10R/siRNA 50:1', n=2 for group of 'NGR-10R/siRNA 20:1'.

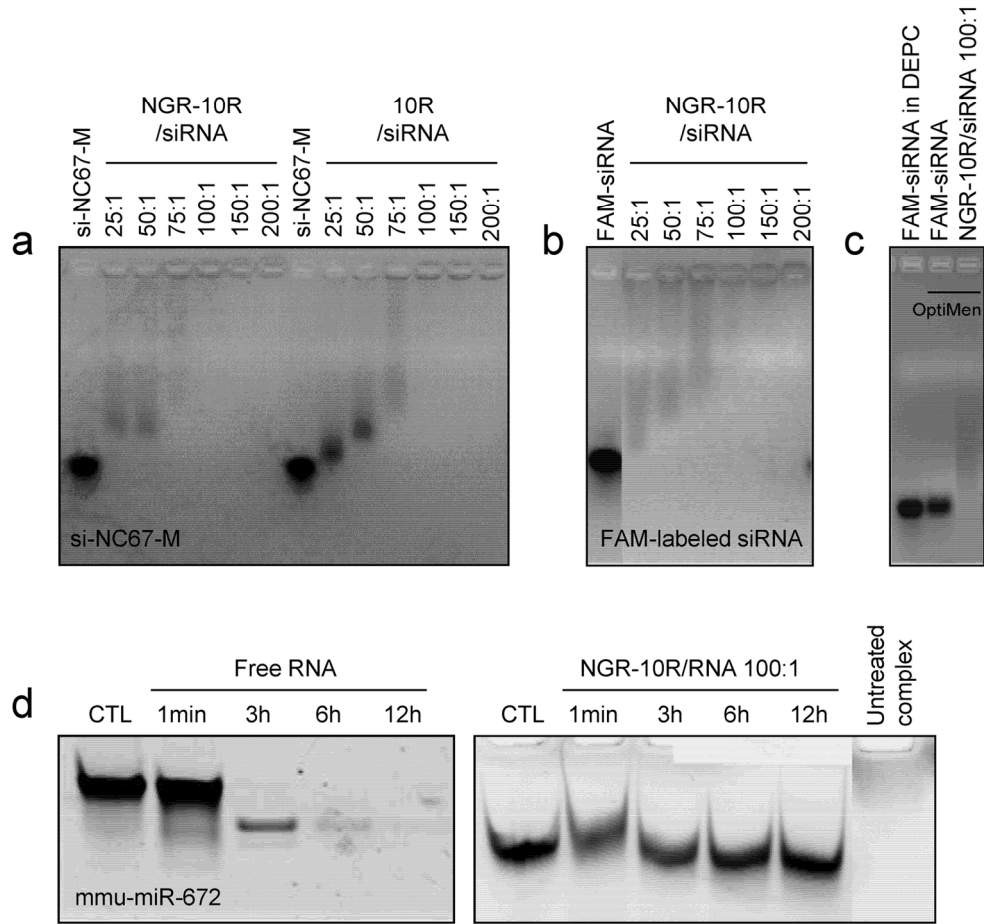
Fig. 7 Tumor-targeted siRNA delivery mediated by NGR-10R/siRNA complexes at 2.5 mg/kg. (a) Whole body imaging at given time points post intravenous injection. (b) Fluorescence images of siRNA accumulated in isolated tissues of BALB/c nude mice at 24 h. (c) Quantification of siRNA accumulated in tissues including tumors. The data were normalized to the corresponding tissue(s) from saline-treated animals. (d) Cryosections of tumor tissues observed by confocal microscopy. DAPI and FITC-labeled phalloidin were used to stain nuclei and F actin (to show the rough cell outline), respectively. Scale bar: 20 μm .

Table 1 Physico-chemical properties of NGR-10R/siRNA complexes with various molar ratios. RVG-9dR/siRNA complexes, lipofectamine 2000/siRNA and free siRNA were included as controls. Data were shown as mean \pm SD, n = 4-6. ND: not detectable.

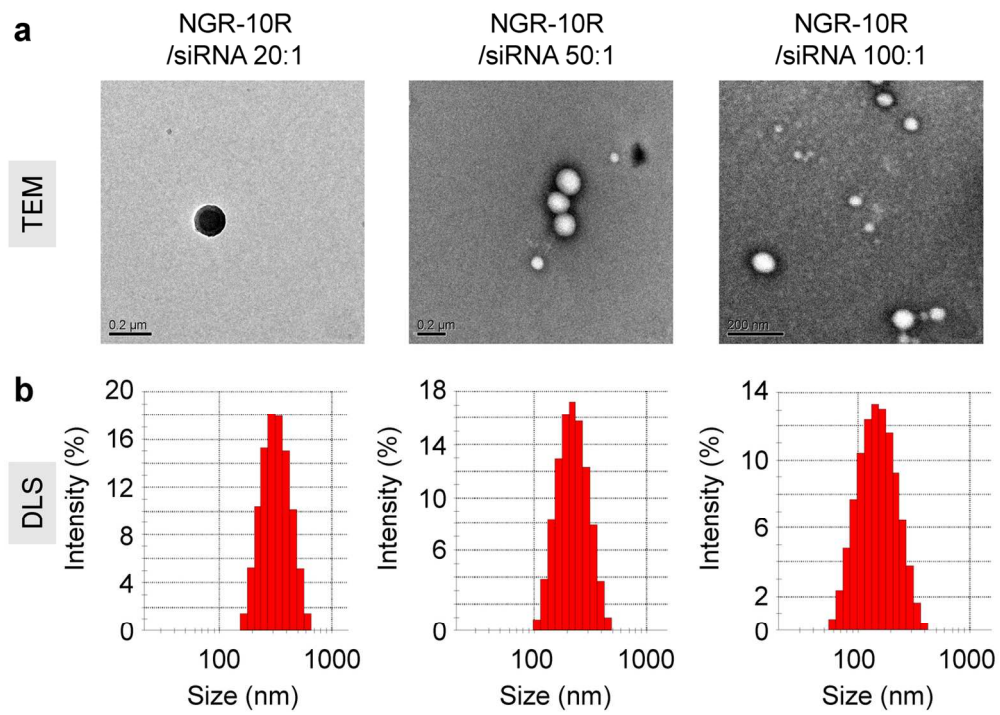
Formulation	Size Distribution		Potential-relative Parameters		
	Size (nm)	PDI	ZP (mV)	Mob ($\mu\text{mcm/Vs}$)	Cond (mS/cm)
NGR-10R/siRNA 20:1	205.0 \pm 94.1	0.225 \pm 0.024	13.05 \pm 2.72	1.025 \pm 0.214	0.0464 \pm 0.0226
NGR-10R/siRNA 50:1	234.7 \pm 58.1	0.284 \pm 0.111	26.13 \pm 16.20	2.048 \pm 1.268	0.0346 \pm 0.0070
NGR-10R/siRNA 100:1	180.8 \pm 32.7	0.296 \pm 0.021	23.28 \pm 15.42	1.825 \pm 1.208	0.0410 \pm 0.0041
RVG-9dR/siRNA 20:1	96.9 \pm 22.7	0.152 \pm 0.060	4.26 \pm 1.12	0.333 \pm 0.088	0.0936 \pm 0.0003
RVG-9dR/siRNA 50:1	66.7 \pm 5.3	0.212 \pm 0.032	6.40 \pm 1.96	0.501 \pm 0.154	0.0649 \pm 0.0011
Lipofectamine 2000/siRNA	140.5 \pm 15.3	0.261 \pm 0.040	24.40 \pm 7.01	1.913 \pm 0.548	0.0498 \pm 0.0271
Naked siRNA	ND	ND	-8.38 \pm 2.54	-0.657 \pm 0.199	0.0418 \pm 0.0232



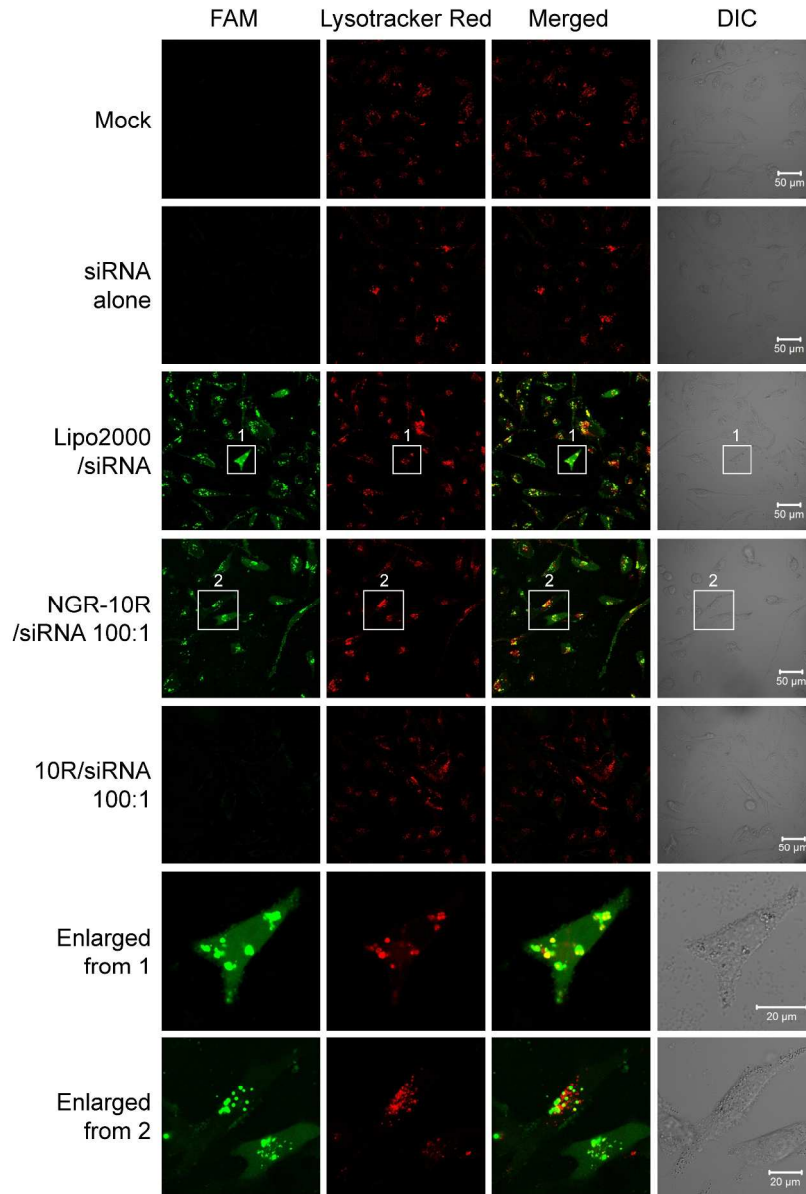
213x216mm (300 x 300 DPI)



143x133mm (300 x 300 DPI)

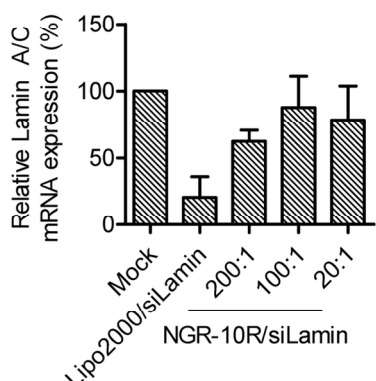


138x101mm (300 x 300 DPI)

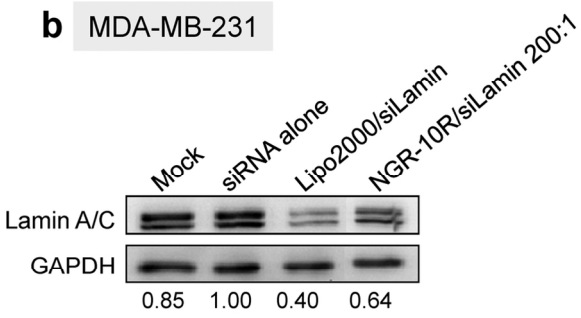


288x425mm (300 x 300 DPI)

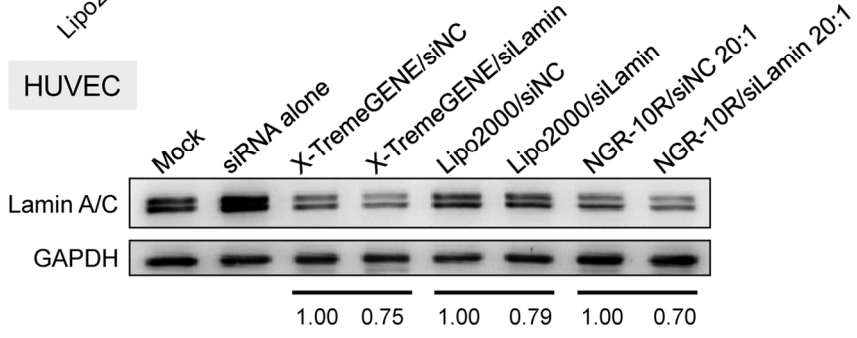
a MDA-MB-231



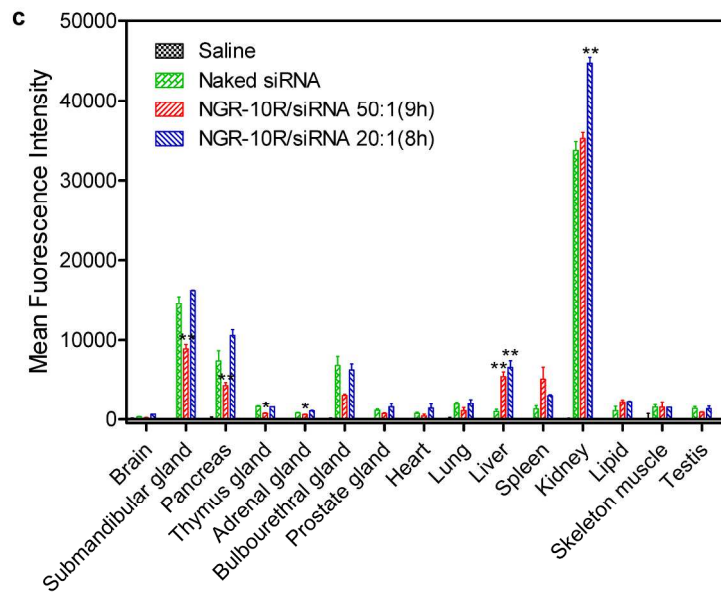
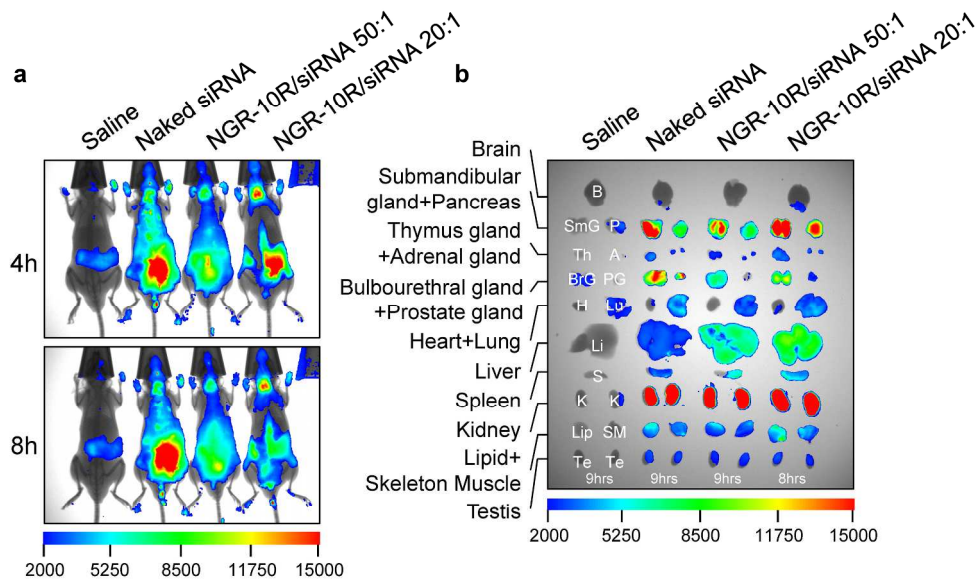
b MDA-MB-231



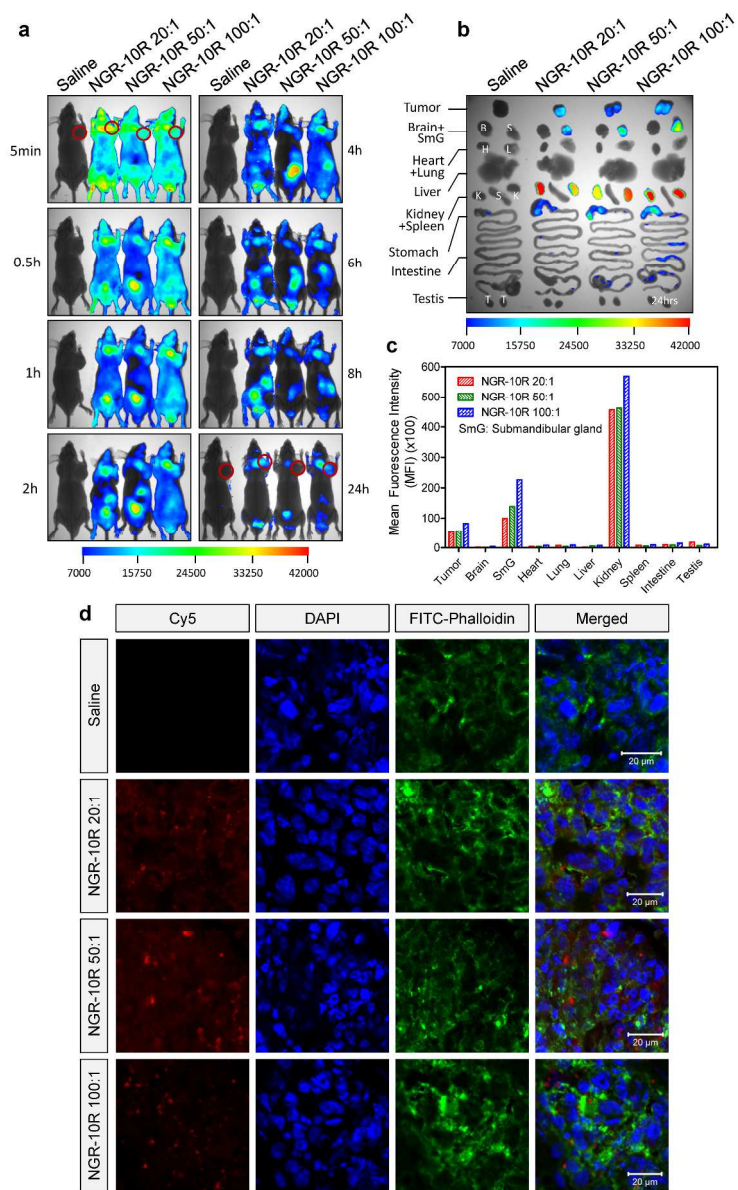
c HUVEC



132x99mm (300 x 300 DPI)



250x304mm (300 x 300 DPI)



297x478mm (300 x 300 DPI)

Benefitting from a thermodynamically-spontaneous and non-enzymatic deamidation reaction, self-assembled NGR-10R/siRNA complex and its isomerization product *iso*DGR-10R/siRNA can recruit CD13 (neovascular) and integrin (neovascular and MDA-MB-231) as their specific receptors. This complex not only efficiently delivered siRNAs into MDA-MB-231 cells *in vitro* but also delivered siRNAs into tumor cells *in vivo*.

